
DEMONSTRATION OF HYBRID DSMC-CFD CAPABILITY FOR NONEQUILIBRIUM REACTING FLOW

Thomas E. Schwartzentruber

**Dept. Aerospace Engineering and Mechanics
University of Minnesota
110 Union St. SE
Minneapolis, MN 55455**

09 February 2018

Final Report

APPROVED FOR PUBLIC RELEASE; DISTRIBUTION IS UNLIMITED.



**AIR FORCE RESEARCH LABORATORY
Space Vehicles Directorate
3550 Aberdeen Ave SE
AIR FORCE MATERIEL COMMAND
KIRTLAND AIR FORCE BASE, NM 87117-5776**

DTIC COPY

NOTICE AND SIGNATURE PAGE

Using Government drawings, specifications, or other data included in this document for any purpose other than Government procurement does not in any way obligate the U.S. Government. The fact that the Government formulated or supplied the drawings, specifications, or other data does not license the holder or any other person or corporation; or convey any rights or permission to manufacture, use, or sell any patented invention that may relate to them.

This report is the result of contracted fundamental research which is exempt from public affairs security and policy review in accordance with AFI 61-201, paragraph 2.3.5.1. This report is available to the general public, including foreign nationals. Copies may be obtained from the Defense Technical Information Center (DTIC) (<http://www.dtic.mil>).

AFRL-RV-PS-TR-2018-0056 HAS BEEN REVIEWED AND IS APPROVED FOR PUBLICATION IN ACCORDANCE WITH ASSIGNED DISTRIBUTION STATEMENT.

//SIGNED//

//SIGNED//

Dr. Thomas Fraser
Program Manager, AFRL/RVBY

Dr. Thomas R. Caudill, Chief
AFRL Battlespace Environment Division

This report is published in the interest of scientific and technical information exchange, and its publication does not constitute the Government's approval or disapproval of its ideas or findings.

REPORT DOCUMENTATION PAGE

Form Approved
OMB No. 0704-0188

Public reporting burden for this collection of information is estimated to average 1 hour per response, including the time for reviewing instructions, searching existing data sources, gathering and maintaining the data needed, and completing and reviewing this collection of information. Send comments regarding this burden estimate or any other aspect of this collection of information, including suggestions for reducing this burden to Department of Defense, Washington Headquarters Services, Directorate for Information Operations and Reports (0704-0188), 1215 Jefferson Davis Highway, Suite 1204, Arlington, VA 22202-4302. Respondents should be aware that notwithstanding any other provision of law, no person shall be subject to any penalty for failing to comply with a collection of information if it does not display a currently valid OMB control number. **PLEASE DO NOT RETURN YOUR FORM TO THE ABOVE ADDRESS.**

1. REPORT DATE (DD-MM-YYYY) 09-02-2018		2. REPORT TYPE Final Report		3. DATES COVERED (From - To) 01 Oct 2017 – 09 Nov 2017	
4. TITLE AND SUBTITLE Demonstration of Hybrid DSMC-CFD Capability for Nonequilibrium Reacting Flow				5a. CONTRACT NUMBER	
				5b. GRANT NUMBER FA9453-17-1-0101	
				5c. PROGRAM ELEMENT NUMBER 62601F	
6. AUTHOR(S) Thomas E. Schwartzentruer				5d. PROJECT NUMBER 1010	
				5e. TASK NUMBER PPM00023729	
				5f. WORK UNIT NUMBER EF129326	
7. PERFORMING ORGANIZATION NAME(S) AND ADDRESS(ES) Dept. Aerospace Engineering and Mechanics University of Minnesota 110 Union St. SE Minneapolis, MN 55455				8. PERFORMING ORGANIZATION REPORT NUMBER	
9. SPONSORING / MONITORING AGENCY NAME(S) AND ADDRESS(ES) Air Force Research Laboratory Space Vehicles Directorate 3550 Aberdeen Avenue SE Kirtland AFB, NM 87117-5776				10. SPONSOR/MONITOR'S ACRONYM(S) AFRL/RVBY	
				11. SPONSOR/MONITOR'S REPORT NUMBER(S) AFRL-RV-PS-TR-2018-0056	
12. DISTRIBUTION / AVAILABILITY STATEMENT Approved for public release; distribution is unlimited.					
13. SUPPLEMENTARY NOTES					
14. ABSTRACT New direct simulation Monte-Carlo (DSMC) and computational fluid dynamic (CFD) models were developed for integration into MGDS and US3D simulation codes. The models are based on new ab-initio rate data obtained using state-of-the-art potential energy surfaces for air species. A probability model (cross-section model) is developed for use in DSMC, and the model analytically integrates to a closed-form model for use in CFD. The model includes the coupling between nonequilibrium (non-Boltzmann) internal energy distributions and dissociation. CFD simulations of the Hollow Cylinder Flare geometry were performed, which involves high-enthalpy flow over a sharp leading edge. Conditions matched recent experiments performed in the CUBRC Lens-XX facility. This flow was chosen since a recent blind-code validation exercise revealed differences in CFD predictions and experimental data that could be due to rarefied flow effects. The CFD solutions (using the US3D code) were run with no-slip boundary conditions and with slip boundary conditions.					
15. SUBJECT TERMS Direct Simulation Monte Carlo, DSMC, computational fluid dynamics, CFD, hypersonic					
16. SECURITY CLASSIFICATION OF:			17. LIMITATION OF ABSTRACT	18. NUMBER OF PAGES	19a. NAME OF RESPONSIBLE PERSON
a. REPORT Unclassified	b. ABSTRACT Unclassified	c. THIS PAGE Unclassified			Dr. Thomas Fraser
			Unlimited	28	19b. TELEPHONE NUMBER (include area code)

This page is intentionally left blank.

Approved for public release; distribution is unlimited.

Table of Contents

List of Figures	ii
1 Summary of Accomplishments.....	1
2 Dissociation Rate Constant Formulation.....	3
3 DSMC and CFD Simulations.....	10
References.....	18

List of Figures

Figure 1: Probability of dissociation as a function of vibrational energy given an average rotational energy and translational temperature ($\langle \epsilon_{rot} \rangle / k_B = T$).....	5
Figure 2: Probability of dissociation as a function of rotational energy given an average vibrational energy and translational temperature.....	5
Figure 3: Rate constant results corresponding to $\langle \epsilon_{rot} \rangle / k_B = T$	8
Figure 4: Comparison of a DMS [3] solution with DSMC. For dissociation and excitation, the TCE model [6] and Millikan and White [7] relaxation times with the high temperature correction are used.	11
Figure 5: Comparison of a DMS [3] solution with DSMC. In DSMC, for dissociation and excitation, the TCE model and DMS based [3] characteristic times have been used respectively.	12
Figure 6: Comparison of a DMS [3] solution with DSMC. In DSMC, for dissociation and excitation, ab initio [8] based models and DMS based characteristic times are used respectively.	13
Figure 7: Hollow cylinder flare geometry and computational setup.	14
Figure 8: Heat flux along the initial cylinder portion of the HCF.....	15
Figure 9: Velocity profiles along the cylinder portion of the HCF geometry.....	16
Figure 10: Temperature profiles along the cylinder portion of the HCF geometry.	17

ACKNOWLEDGMENTS

This material is based on research sponsored by Air Force Research Laboratory under agreement number FA9453-13-1-0292. The U.S. Government is authorized to reproduce and distribute reprints for Governmental purposes notwithstanding any copyright notation thereon.

DISCLAIMER

The views and conclusions contained herein are those of the authors and should not be interpreted as necessarily representing the official policies or endorsements, either expressed or implied, of Air Force Research Laboratory or the U.S. Government.

This page is intentionally left blank.

Approved for public release; distribution is unlimited.

1 Summary of Accomplishments

The Statement of Work for this project involved four main tasks. The tasks are repeated here along with a short summary of the research accomplishments and publications for each task. More detailed findings are included in the remainder of the report.

(1) *“Implement the new dissociation model into both DSMC and CFD codes.”*

New DSMC and CFD models were developed for integration into MGDS and US3D simulation codes. The models are based on new ab-initio rate data obtained using state-of-the-art potential energy surfaces (PESs) for air species. A probability model (cross-section model) is developed for use in DSMC, and the model analytically integrates to a closed-form model for use in CFD. The model includes the coupling between nonequilibrium (non-Boltzmann) internal energy distributions and dissociation.

The model for nonequilibrium internal energy distributions is published in the Proceedings of the National Academy of Sciences, a very high impact-factor journal:

Singh, N. and Schwartzentruber, T.E., “Nonequilibrium internal energy distributions during dissociation”, *Proceedings of the National Academy of Sciences* (2018) 115 (1) 47-52; published ahead of print December 18, 2017.

The DSMC and CFD models are published in AIAA conference proceedings:

Singh, N. and Schwartzentruber, T.E., “Coupled Vibration-Rotation Dissociation Model for Nitrogen from Direct Molecular Simulations”, *AIAA Paper 2017-3490*, presented at the 47th AIAA Thermophysics Conference, Aviation Forum, Denver, CO.

(2) *“Perform full CFD simulations of a candidate nonequilibrium flow (for example a sharp leading edge flow).”*:

CFD simulations of the Hollow Cylinder Flare (HCF) geometry were performed, which involves high-enthalpy flow over a sharp leading edge. Conditions matched recent experiments performed in the CUBRC Lens-XX facility. This flow was chosen since a recent blind-code validation exercise revealed differences in CFD predictions and experimental data that could be due to rarefied flow effects. The CFD solutions (using the US3D code) were run with no-slip boundary conditions and with slip boundary conditions. Interestingly, the results showed that even though slip effects are present, the heat flux predicted by both slip and no-slip calculations was virtually identical. This was found to be caused by increased shear-work (increased energy transfer to the surface) due to non-zero velocity at the wall, which compensates for the reduced

temperature gradient.

(3) *“Perform full DSMC simulations of the same candidate flow (for example a sharp leading edge flow). Pure CFD and DSMC solutions will be compared for different degrees of continuum vs. rarefied flow. Demonstrate consistency between pure DSMC and CFD solutions for a chemically reacting flow under continuum conditions.”*:

DSMC simulations of the same HCF flow were performed using the MGDS code. DSMC naturally predicts slip flow and temperature-jump near the wall. Slip effects were indeed present, and differed noticeably with the slip predicted by CFD. However, the overall heat flux predicted by DSMC was in excellent agreement with that predicted by CFD. This implies that the difference between CFD predictions and experimental data is not due to rarefied flow and slip effects.

The DSMC and CFD simulation results, comparisons with experimental data, and detailed analysis of slip flow, are published in AIAA conference proceedings (and are in preparation for submission to the AIAA journal):

Bhide, P., Singh, N., Nompelis, I., Schwartzentruber, T.E., and Candler, G.V., “Slip effects in near continuum hypersonic flow over canonical geometries”, *AIAA Paper 2018-1235*, presented at the AIAA SciTech Forum, Kissimmee, FL.

(4) *“For conditions where DSMC is required in only a sub-region of the flow, use boundary conditions provided from a CFD solution to a small DSMC simulation of only the sub-region. Compare the hybrid solution to pure DSMC and ensure that the solutions are consistent. Perform pure CFD, pure DSMC, and hybrid solutions of other candidate flows.”*:

While the remarkable agreement between DSMC and CFD was a successful demonstration for a reacting flow under continuum conditions, it also meant that this HCF flow was not an ideal candidate to demonstrate a hybrid CFD-DSMC solution. Furthermore, this test case revealed that coupling CFD to DSMC near surfaces represents an additional challenge (not foreseen in the initial proposal). Specifically, there were noticeable differences between the near-wall flow field properties. Such differences need to be addressed (perhaps by a new slip model in CFD) before a hybrid capability can be fully realized.

The remainder of the report contains a detailed description of the project findings.

2 Dissociation Rate Constant Formulation

The most general expression for the rate constant k , under the assumption that the internal energy of the molecule is separable, is the following [1]:

$$k(\langle \epsilon_{rel} \rangle, \langle \epsilon_{rot} \rangle, \langle \epsilon_v \rangle) = \frac{1}{S} \sum_{v=0}^{v_{max}} \sum_{j=0}^{j_{max}} \int_0^{\infty} \sigma(\epsilon_{rel}, \epsilon_{rot}, \epsilon_v) v_{rel} f(v_{rel}) dv_{rel} f(\epsilon_{rot}) f(\epsilon_v) \quad (1)$$

where, $\sigma(\epsilon_{rel}, \epsilon_{rot}, \epsilon_v)$ is the reaction cross-section averaged over impact parameter, v_{rel} is relative speed, ϵ_{rot} and ϵ_v are the rotational and vibrational energy of the molecule undergoing dissociation, and S is the symmetry factor. $f(v_{rel})$ is the probability density function of relative speed, $f(\epsilon_{rot})$ is the probability distribution for rotational energy, and $f(\epsilon_v)$ is the probability distribution for vibrational energy. Our model can be obtained assuming equilibrium internal energy distribution functions, however, can also be formulated using non-equilibrium (non-Boltzmann) internal energy distribution functions.

2.1 DSMC Model: Reaction Cross Section, $\sigma(\epsilon_{rel}, \epsilon_{rot}, \epsilon_v)$

The reaction cross-section is equivalent to the probability used in the DSMC method:

$$p(d|\epsilon_{rel}, \epsilon_{rot}, \epsilon_v) = \frac{\sigma(\epsilon_{rel}, \epsilon_{rot}, \epsilon_v)}{\pi b_{max}^2} \quad (2)$$

where b_{max} is maximum impact parameter used to generate the ab-initio collision database (via Quasi-Classical Trajectory Calculations, QCT or Direct Molecular Simulations, DMS).

Instead of finding this three dimensional probability, which has a huge parameter space, we average this probability over the other two energy modes. For instance, integrating this probability over translational and rotational energy, results in its dependence only on vibrational energy. This dependence is shown in Fig. 1. The dependence of dissociation probability on vibrational energy is clearly exponential. The probability of dissociation on rotational energy (averaged over translational and vibrational energy) is shown in Fig. 2. This dependence is also exponential. Although not shown, the dependence on translational energy has similar clear trends. We observe such simple trends for different air species (nitrogen and oxygen) and for different collision partners (atoms vs. molecules).

Based on these trends revealed by ab-initio calculations, we propose the following form for

$p(d|\epsilon_{rel}, \epsilon_{rot}, \epsilon_v)$:

$$p(d | \epsilon_{rel}, \epsilon_v, \epsilon_{rot}) = C_1 \overbrace{\left[\frac{\epsilon_{rel} + \epsilon_{int} - \epsilon_d}{\epsilon_d} \right]^\alpha}^{\text{I}} \overbrace{\frac{\epsilon_d}{\epsilon_{rel}} \exp \left[\beta \frac{\epsilon_{rot}}{\epsilon_d} \right]}^{\text{II}} \overbrace{\exp \left[\gamma \frac{\epsilon_v}{\epsilon_d} \right]}^{\text{III}}, \quad \begin{array}{l} \epsilon_{rel} + \epsilon_{int} \geq \epsilon_d \\ \epsilon_{rel} + \epsilon_{int} < \epsilon_d \end{array} \quad (3)$$

$$= 0,$$

where $C_1 = 7.5 \times 10^{-3}$, $\alpha = 1.80$, $\beta = 0.50$, $\gamma = 2.50$.

- **Term I** captures the dependence of dissociation probability on relative translational energy, with the product of two terms. The first quantifies how far the molecular system is from the required dissociation energy. The closer it is, the higher the probability, and vice-versa. The second term appears due to the decrease in probability (reaction-cross section) when relative translational energy is too high and “fly-by” collisions are more frequent (Note that $\alpha > 1.0$).
- **Term II** quantifies the dependence of dissociation probability on rotational energy with parameter β .
- **Term III** quantifies the dependence of dissociation probability on vibrational energy with parameter γ .

The parameters α , β , and γ , capture the relative importance of translational, rotational, and vibrational energy for the dissociation probability. The new model results are shown by the lines in Figs. 1 and 2, where good agreement is seen with the ab-initio cross-section data. Obviously, the model does not fit the data precisely, however, the reduction of millions of state-to-state transition probabilities to a simple model function is required for tractable DSMC and CFD models. In the next section, it will be shown that this probability function allows for analytical integration in the limit of continuum flow, resulting in a closed-form model for CFD.

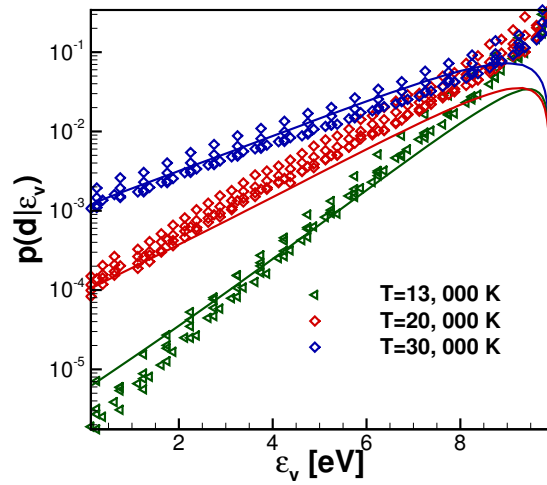


Figure 1: Probability of dissociation as a function of vibrational energy given an average rotational energy and translational temperature ($\langle \epsilon_{rot} \rangle / k_B = T$). The rotational and translational energies are assumed to have Boltzmann distributions (consistent with the underlying QCT data). The new model is shown with solid lines.

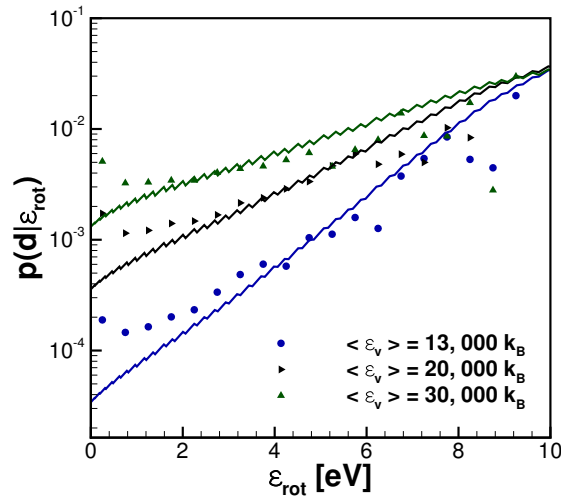


Figure 2: Probability of dissociation as a function of rotational energy given an average vibrational energy and translational temperature. The translational energies are assumed to have Boltzmann distributions (consistent with the underlying QCT data) at 30,000 K. The new model is shown with solid lines.

2.2 CFD Model: Assuming Boltzmann Internal Energy Distributions

By plugging-in Boltzmann (equilibrium) distribution functions for $f(\epsilon_{rot})$ and $f(\epsilon_v)$ in Eq. 1, the following rate constant can be obtained analytically (see AIAA Paper 2017-3490 by Singh and Schwartzentruber for full details):

$$k(T, \langle \epsilon_{rot} \rangle, \langle \epsilon_v \rangle) = AT^\eta \exp \left[-\frac{\epsilon_d}{k_B T} \right] * G_{rot} * G_v \quad (4)$$

$$\eta = \frac{1}{2} + \alpha - 1 = \alpha - \frac{1}{2}$$

$$A = \frac{1}{S} \left(\frac{8k_B}{\pi\mu_C} \right)^{1/2} \pi b_{\max}^2 C_1 \Gamma[1 + \alpha] \left(\frac{k_B}{\epsilon_d} \right)^{\alpha-1}$$

where, k_B is Boltzmann constant, T is translational temperature, and ϵ_d is the bond dissociation energy of the nitrogen molecule. G_{rot} and G_v are functions that result from the integration, which capture the dependence on rotational and vibrational energy. Therefore, the model has a standard modified Arrhenius form based on the gas translational temperature, but now contains two separate controlling functions that modify the rate due to the local rotational and vibrational energy state of the gas. This is in contrast to the Park model that uses an empirical effective temperature $T_{eff} = \sqrt{T T_v}$ within the Arrhenius expression; a form not derivable from kinetic theory and inconsistent with recent ab-initio data.

It is important to note that G_{rot} and G_v are only a function of average internal energy values and the translational temperature. Such average quantities are already tracked in multi-temperature CFD codes. Therefore, the model can be incorporated with little additional cost within state-of-the-art hypersonic CFD codes.

The functions G_{rot} and G_v are given by:

$$G_{rot} = \frac{\overbrace{\exp [j_{\max}(j_{\max} + 1)\delta_{rot}] - 1}^{A_{rot}}}{\delta_{rot}} \overbrace{\frac{\langle \epsilon_{rot} \rangle}{\eta_{rot}\theta_r k_B}}^{B_{rot}}, \quad \delta_{rot} \neq 0$$

$$= j_{\max}(j_{\max} + 1) \frac{\langle \epsilon_{rot} \rangle}{\eta_{rot}\theta_r k_B}, \quad \delta_{rot} = 0 \quad (5)$$

$$\rightarrow \delta_{rot} = \eta_{rot}\theta_{rot}k_B \left(-\frac{1}{\langle \epsilon_{rot} \rangle} + \beta \frac{1}{\epsilon_d} + \frac{1}{k_B T} \right)$$

$$\begin{aligned}
G_v &= \exp \left[\overbrace{\left[\frac{\delta_v}{2} \right]}^{A_v} \frac{1 - \exp[\delta_v v_{\max}]}{1 - \exp[\delta_v]} \overbrace{\frac{1 - \exp[-\theta_v k_B / \langle \epsilon_v \rangle]}{\exp[-\theta_v k_B / (2\langle \epsilon_v \rangle)]}}^{B_v} \right], & \delta_v \neq 0 \\
&= v_{\max} \frac{1 - \exp[-\theta_v k_B / \langle \epsilon_v \rangle]}{\exp[-\theta_v k_B / (2\langle \epsilon_v \rangle)]}, & \delta_v = 0 \\
&\rightarrow \delta_v = \theta_v k_B \left(-\frac{1}{\langle \epsilon_v \rangle} + \gamma \frac{1}{\epsilon_d} + \frac{1}{k_B T} \right)
\end{aligned} \tag{6}$$

Here, θ_{rot} is the characteristic rotational temperature, θ_v is the characteristic vibrational temperature, $\langle \epsilon_{rot} \rangle$ and $\langle \epsilon_v \rangle$ are the average rotational and vibrational energies (known in each cell of a multi-temperature CFD simulation). Many of the exponential terms seen in Eqs. 5 and 6 result from the equilibrium internal energy distribution functions used for integration. Specifically, to perform analytical integration, we need the variation of rotational and vibrational energy with the *quantized* rotation and vibration levels. The following points are considered:

- We modify the rigid rotor model by η_{rot} , and use the truncated harmonic oscillator model for vibration. j_{max} and v_{max} are consequently the maximum allowed rotational and vibrational level, consistent with quantum mechanics data. Although these are approximations to the true equilibrium distribution functions, we propose that these simple models are sufficiently accurate. Furthermore, in the next section we integrate over nonequilibrium distribution functions, which alters the integration process further.
- In G_{rot} (or G_v), the term B_{rot} (or B_v) quantifies the the dependence of the probability of dissociation on average rotational (or vibrational) energy. This term is independent of the parameter β (or γ). This represents the contribution of internal energy to the total collision energy in comparison to the dissociation energy; a consequence of ‘I’ in Eq. 3.
- The term A_{rot} (or A_v) in G_{rot} (or G_v), depends on the parameter β (or γ), and is proportional to δ_{rot} (or δ_v). At a given translational temperature, δ_{rot} (or δ_v) captures the *relative* dependence of rotation (or vibration), through the parameter β (or γ). This dependence includes the effective population of internal energies captured by $-1/\langle \epsilon_{rot} \rangle$ (or $-1/\langle \epsilon_v \rangle$). As described in the next section, when integrating over non-Boltzmann internal energy distributions, it is only this term that is affected, since the population of high internal energy levels can be overpopulated or depleted.

Although the functions G_{rot} and G_v appear complicated with many parameters, it is important to note that they are derived analytically from the DSMC (cross-section) model and no new parameters are introduced. The new model results (Eq. 4) are compared with the

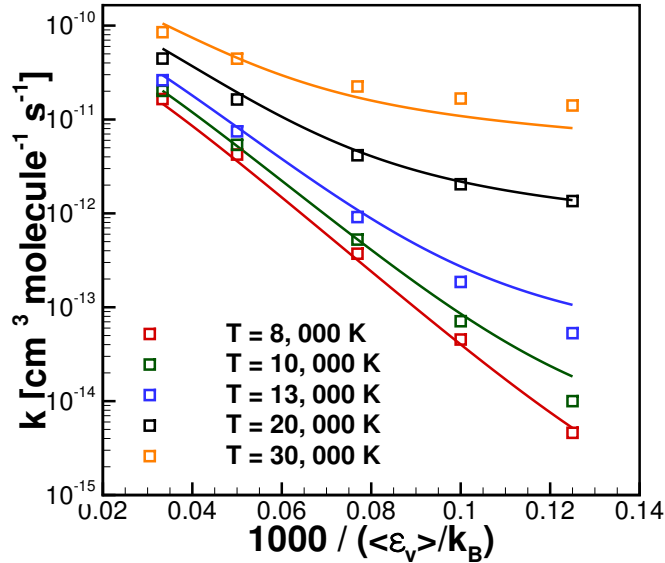


Figure 3: Rate constant results corresponding to $\langle \epsilon_{rot} \rangle / k_B = T$. Square symbols represent QCT data, while solid lines correspond to the new model in Eq. 4.

QCT results of Bender et al. [2] in Fig. 3. Recall that the QCT data was obtained assuming Boltzmann distributions at the corresponding temperatures and, since our model also integrates over Boltzmann distribution functions, good agreement is expected. Again, the agreement is not exact, but very good for such a simplified model. We now proceed to formulate the model using non-Boltzmann internal energy distribution functions.

2.3 CFD Model: Using Non-Boltzmann Internal Energy Distributions

Hypersonic flows of interest involve nonequilibrium distributions of internal energy. To date, such effects have been captured by empirical models fit to limited experimental data. However, while such empirical models will reproduce the experimental data they were fit to, their accuracy is uncertain for conditions outside of these limited conditions. This is why so much effort has gone into the development of state-resolved models and binned-state-resolved models. Such modeling can predict non-Boltzmann populations of internal energy and their coupling to dissociation and, therefore, should be more accurate for highly-nonequilibrium conditions beyond existing experimental conditions. The main challenge associated with resolving non-Boltzmann populations of internal energies is that the number of degrees of freedom (variables one must

compute and track) becomes quickly intractable. While this research is important, the approach we have taken with support from this grant is to create a simple model that captures the key non-Boltzmann effects. The results were recently published in PNAS [5]. Please refer to the journal article for full details.

To summarize, the key non-Boltzmann physics include: (1) During rapid rovibrational excitation behind a strong shock wave, the high-energy tails of the internal energy distribution functions become *overpopulated* compared to the Boltzmann distribution based on the average energy. (2) During significant dissociation, the high-energy molecules are depleted (due to dissociation) more rapidly than they can be replenished by internal energy excitation. This *depletion* reduces the dissociation rate compared to the Boltzmann assumption. These are the two key physical mechanisms that should be captured by a new dissociation model [3, 4].

Our new model for nonequilibrium internal energy distribution functions is:

$$f(i) = C_{1,i} f_0(i) \times \overbrace{\exp \left[-\lambda_{1,i} \frac{\langle \epsilon_t \rangle}{\epsilon_d} \Gamma_i \right]}^{D_i} \times \overbrace{\exp \left[-\lambda_{2,i} \left(\frac{2 \langle \epsilon_t \rangle}{3 \langle \epsilon_i \rangle} - \frac{3 \langle \epsilon_i \rangle}{2 \langle \epsilon_t \rangle} \right) \Gamma_i \right]}^{O_i}, \quad (7)$$

where i corresponds to the internal mode ($i \rightarrow v$ or j), $\Gamma_v = v$, $\Gamma_j = j(j+1)$, and $f_0(i)$ is a Boltzmann distribution. Therefore, both overpopulation (O_i) and depletion (D_i) terms model the departure from an equilibrium (Boltzmann) distribution. We found that these terms can be accurately modeled as surprisal functions that are linear in v , or $j(j+1)$.

Specifically, it is the translational energy $\langle \epsilon_t \rangle / \langle \epsilon_d \rangle$ that controls the depletion due to dissociation (D_i), whereas the energy gap $\langle \epsilon_t \rangle - \langle \epsilon_i \rangle$ controls the overpopulation during rapid excitation (O_i). The four model parameters ($\lambda_{1,i}$ and $\lambda_{2,i}$) are used to fit the overpopulation and depletion of both rotation and vibrational energies, and are determined from the ab initio DMS results.

Now, one can integrate the rate equation using accurate nonequilibrium internal energy distributions (Eq. 7). The result is the same as that presented above, with only a small change in the functions G_v and G_{rot} . In fact, only δ_v and δ_{rot} expressions change:

$$\begin{aligned} \delta_v &= \theta_v k_B \left[-\frac{1}{\langle \epsilon_v \rangle} + \gamma \frac{1}{\epsilon_d} + \frac{1}{k_B T} + \delta_v^{NE} \right] \\ \delta_v^{NE} &= -\lambda_{1,v} \frac{\langle \epsilon_t \rangle}{\epsilon_d} - \lambda_{2,v} \left(\frac{2 \langle \epsilon_t \rangle}{3 \langle \epsilon_v \rangle} - \frac{3 \langle \epsilon_v \rangle}{2 \langle \epsilon_t \rangle} \right) \end{aligned}$$

$$\delta_{rot} = \eta_{rot} \theta_{rot} k_B \left[-\frac{1}{\langle \epsilon_{rot} \rangle} + \beta \frac{1}{\epsilon_d} + \frac{1}{k_B T} + \delta_{rot}^{NE} \right]$$

$$\delta_{rot}^{NE} = -\lambda_{1,rot} \frac{\langle \epsilon_t \rangle}{\epsilon_d} - \lambda_{2,rot} \left(\frac{2}{3} \frac{\langle \epsilon_t \rangle}{\langle \epsilon_{rot} \rangle} - \frac{3}{2} \frac{\langle \epsilon_{rot} \rangle}{\langle \epsilon_t \rangle} \right)$$

In this manner, the magnitude of G_{rot} and G_v not only adjust the dissociation rate due to the average rotational and vibrational energy of the gas, but also includes an estimate of the effect due to non-Boltzmann populations. The model is simple (compared to state-resolved and binned models), it can fit within a multi-temperature CFD framework, and it is analytically consistent with the corresponding DSMC model. Notice that by setting $\delta_i^{NE} = 0$, one recovers the equilibrium dissociation rate corresponding to Boltzmann internal energy distributions. The new model parameters (α , β , and γ) capture the relative influence of translation, rotation, and vibration on dissociation, while the parameters ($\lambda_{1,i}$ and $\lambda_{2,i}$) capture the influence of overpopulated and depleted high-energy molecules.

3 DSMC and CFD Simulations

3.1 Model Results

In this section we compare DSMC results (using the new model) with the ab-initio Direct Molecular Simulation (DMS) results for the rovibrational excitation and dissociation expected behind strong shock waves. To summarize, we find existing models cannot predict the DMS results, whereas our new model very accurately reproduces DMS dissociation results. In the process we found that the rotational and vibrational energy excitation models also play a crucial role (more crucial than we had originally expected). Therefore our new dissociation model is a large improvement, however, it is important to combine with new models for rovibrational relaxation (on-going).

In Fig. 4 we see that the standard DSMC models (the Total Collision Energy (TCE) model) gets the rotational and vibrational excitation rates wrong, and also gets the dissociation rate wrong, compared to the DMS result.

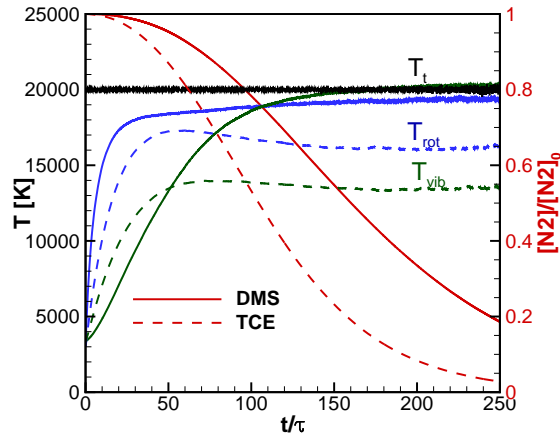


Figure 4: Comparison of a DMS [3] solution with DSMC. For dissociation and excitation, the TCE model [6] and Millikan and White [7] relaxation times with the high temperature correction are used. τ is the mean collision time based on the variable hard sphere model.

In Fig. 5, we see that when we adjust the rotational and vibrational excitation rates, to match DMS, the dissociation rate is still not accurately captured by the standard DSMC TCE model.

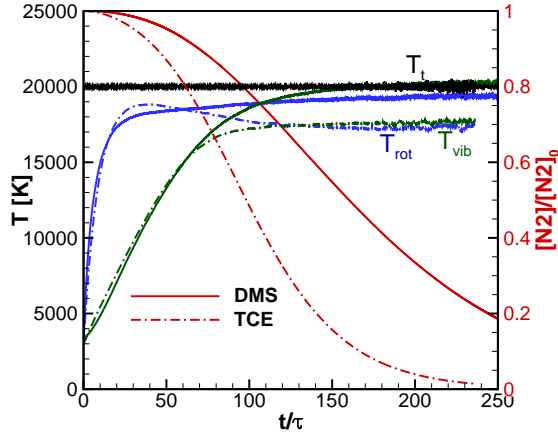


Figure 5: Comparison of a DMS [3] solution with DSMC. In DSMC, for dissociation and excitation, the TCE model and DMS based [3] characteristic times have been used respectively. τ is mean collision time based on variable hard sphere model.

In Fig. 6, we see that when we use adjusted excitation rates and the new DSMC probability model, that we now accurately reproduce the ab initio dissociation process. However, note that we still do not obtain the correct Quasi-Steady-State (QSS). We have determined that simply “adjusting” the excitation rates to match DMS data is not sufficient. Rather, there is a fundamental problem with the standard DSMC internal energy relaxation model that no amount of adjusting can fix. We are in the process of fixing this problem. We did not fully appreciate the importance of this, and it is an important outcome of the current research.

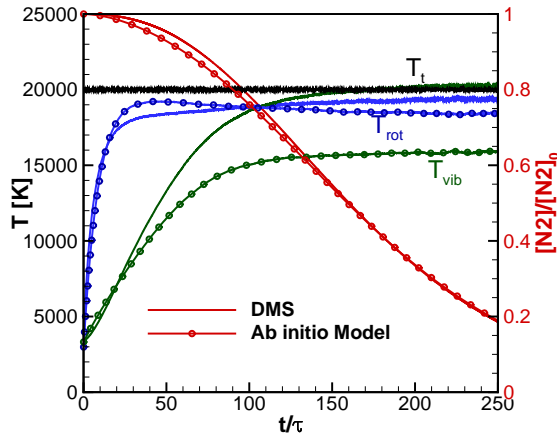


Figure 6: Comparison of a DMS [3] solution with DSMC. In DSMC, for dissociation and excitation, ab initio [8] based models and DMS based characteristic times are used respectively. τ is mean collision time based on the variable hard sphere model.

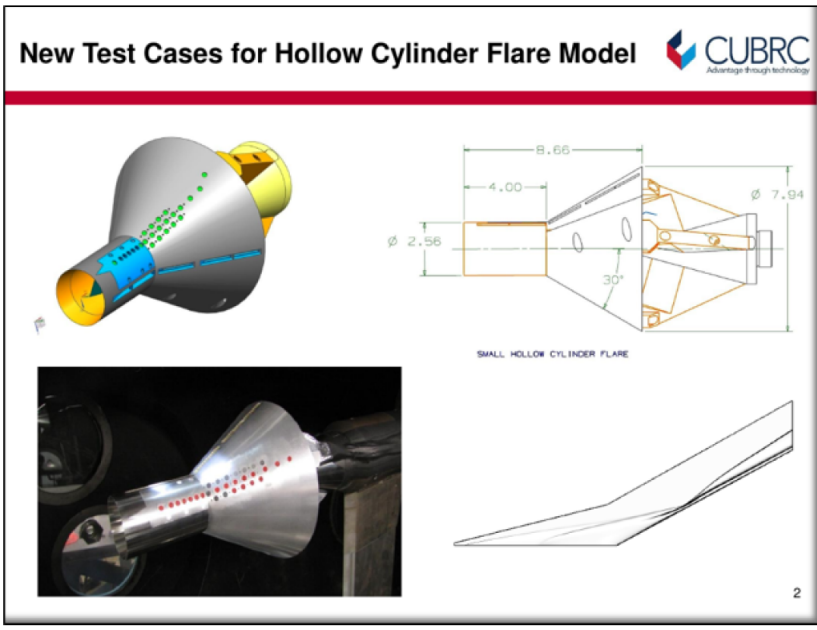
3.2 CFD and DSMC Simulations of Near-Continuum Flows

It is important that DSMC solutions agree with CFD solutions in the limit of near-continuum flow. We performed hypersonic flow simulations for a Hollow Cylinder Flare (HCF) geometry, using the MGDS code, and solutions were compared to CFD results using the US3D code. This test case includes recent experimental data that can be used to validate both DSMC and CFD predictions, and this test case is computationally challenging.

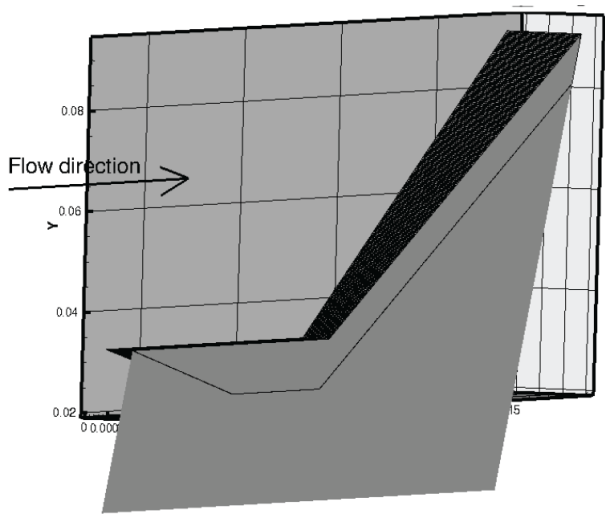
The HCF geometry is shown in Fig. 7(a), which is reproduced from a presentation from the following paper:

MacLean, M., Holden, M., and Dufrene, A., “Comparison Between CFD and Measurements for Real-Gas Effects on Laminar Shock Wave Boundary Layer Interaction’ - 1”, AIAA Aviation, 44th AIAA Fluid Dynamics Conference, 2014.

The conditions align with “Run 1” conditions for the high enthalpy flow experiments performed at CUBRC. Specifically, $V=3123$ m/s, $\rho = 6.1 \times 10^{-4}$ kg/m³, $T=189$ K, and $T_{wall}=300$ K. Since the geometry is axi-symmetric, only a 5 degree wedge is simulated as shown in Fig. 7(b).



(a) HCF geometry.



(b) DSMC simulation setup.

Figure 7: Hollow cylinder flare geometry and computational setup.

One of the results of the blind code-validation exercise (presented in the above paper) was that even on the initial cylinder portion of the geometry, the heat flux predicted by CFD codes did not agree precisely with the experimental data. It was speculated that this could be due to slip-flow effects. This is the main motivation for the simulations summarized here. As seen

in Fig. 8, the heat flux predicted by DSMC (MGDS) is quite close to that predicted by CFD (US3D), and both are noticeably lower than the experimental data. It is important to note that the CFD simulations employed a slip-flow boundary condition. Velocity profiles in the boundary layer are shown at two stations, one near the leading edge of the HCF (Fig. 9(a)) and downstream of the leading edge (Fig. 9(b)). Both DSMC and CFD predict the same degree of slip flow. Note that the velocity is scaled by the freestream velocity in these figures. Also, it is evident that the degree of slip flow decreases as distance from the leading edge increases (station 3 vs. station 1). The temperature profiles at the same stations are shown in Figs. 10(a) and 10(b). A temperature jump is predicted by both DSMC and CFD, which diminishes as distance downstream increases. Here, more noticeable differences are seen in the boundary layer, however, as seen in the heat flux result (Fig. 8), these differences have little effect on the net heat flux to the surface. Therefore, differences in the boundary layer are evident between DSMC and CFD as expected for this near-continuum flow, however, the net effect on the surface is negligible and both methods are in close agreement.

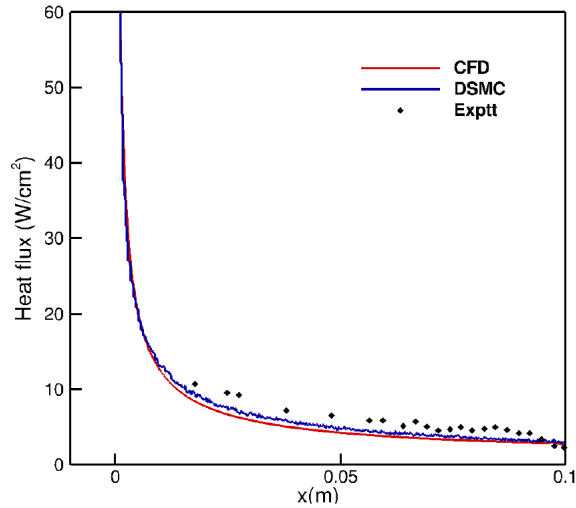
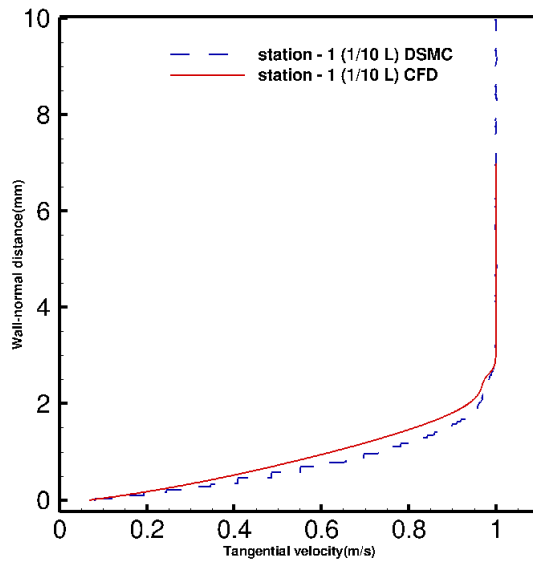
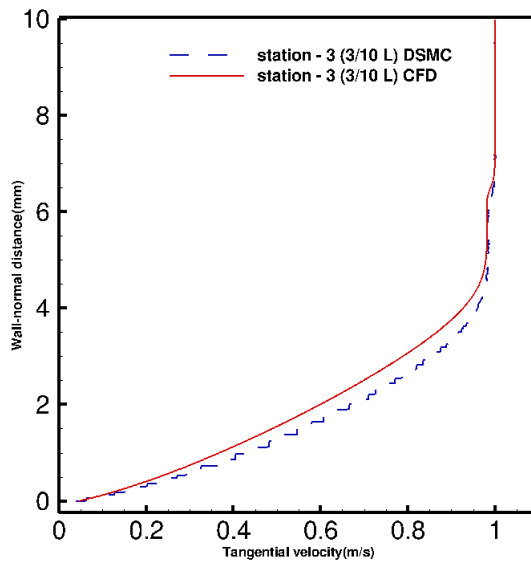


Figure 8: Heat flux along the initial cylinder portion of the HCF.

Full details of this research, were presented at the AIAA SciTech conference in January of 2018 (refer to publication listing in the introduction).

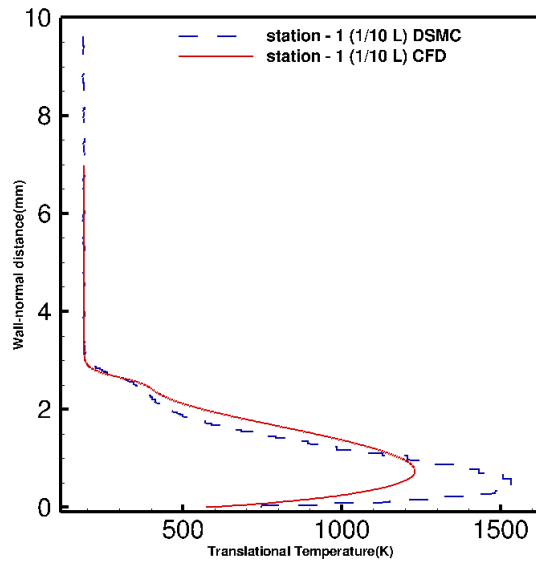


(a) Station 1 near the leading edge.

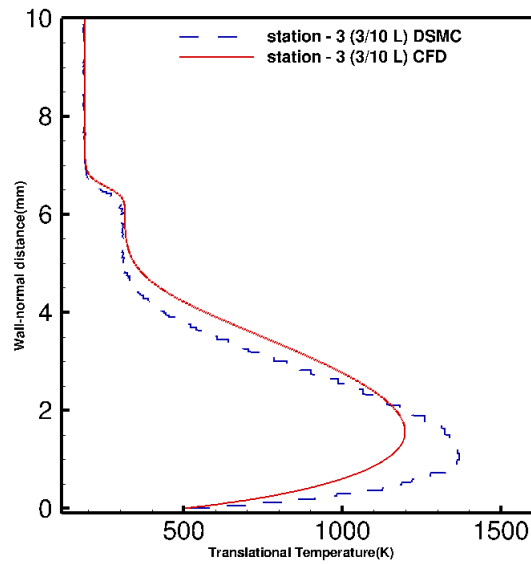


(b) Station 3 downstream of the leading edge.

Figure 9: Velocity profiles along the cylinder portion of the HCF geometry.



(a) Station 1 near the leading edge.



(b) Station 3 downstream of the leading edge.

Figure 10: Temperature profiles along the cylinder portion of the HCF geometry.

References

- [1] J. T. Muckerman, D. G. Truhlar, and R. B. Bernstein, Atom–Molecule Collision Theory: A Guide for the Experimentalist, Plenum, New York, 1979.
- [2] Jason D. Bender, Paolo Valentini, Ioannis Nompelis, Yuliya Paukku, Zoltan Varga, Donald G. Truhlar, Thomas Schwartzentruber, and Graham V Candler, "An Improved Potential Energy Surface and Multi-Temperature Quasiclassical Trajectory Calculations of $N_2^+ + N_2$ Dissociation Reactions," *The Journal of Chemical Physics*, 143(5):054304, 2015.
- [3] Paolo Valentini, Thomas E. Schwartzentruber, Jason D. Bender, and Graham V. Candler, "Dynamics of Nitrogen Dissociation from Direct Molecular Simulation," *Physical Review Fluids*, 1(4):043402, 2016.
- [4] Paolo Valentini, Thomas E. Schwartzentruber, Jason D. Bender, Ioannis Nompelis, and Graham V. Candler, "Direct Molecular Simulation of Nitrogen Dissociation Based on an ab initio Potential Energy Surface," *Physics of Fluids*, 27(8):086102, 2015.
- [5] Narendra Singh and Thomas Schwartzentruber, "Nonequilibrium Internal Energy Distributions During Dissociation," *Proceedings of the National Academy of Sciences*, 115(1):47–52, 2018.
- [6] G. A. Bird, "Monte-Carlo Simulation in an Engineering Context," *Progress in Astronautics and Aeronautics*, 74:239–255, 1981.
- [7] Roger C. Millikan and Donald R. White, "Systematics of Vibrational Relaxation," *The Journal of Chemical Physics*, 39(12):3209–3213, 1963.
- [8] Narendra Singh and Thomas E. Schwartzentruber, "Coupled Vibration-Rotation Dissociation Model for Nitrogen from Direct Molecular Simulations," In *47th AIAA Thermophysics Conference*, Denver, CO, p. 3490, 2017.

DISTRIBUTION LIST

DTIC/OCP 8725 John J. Kingman Rd, Suite 0944 Ft Belvoir, VA 22060-6218	1 cy
AFRL/RVIL Kirtland AFB, NM 87117-5776	1 cy
Official Record Copy AFRL/RVBY/Dr. Thomas Fraser	1 cy

This page is intentionally left blank.